

CHAPTER **7** SEMICONDUCTORS AND
MATERIALS AREA



EFFECT OF DENSITY OF STATES
IN ELECTRICAL SIMULATION
OF AMORPHOUS INDIUM-
GALLIUM-ZINC-OXIDE THIN FILM
TRANSISTOR

**Arturo Torres-Sánchez, Isai Hernández-Luna,
Francisco Hernández-Cuevas, Cuauhtémoc León-Puertos,
Norberto Hernández-Como**

Centro de Nanociencias y Micro y Nanotecnologías, Instituto Politécnico Nacional,
México City, México.

Abstract

Amorphous oxide semiconductors (AOS) used as channel in Thin Film Transistors (TFTs) have extended their applications not only as switching devices in display technologies, but also as main elements in logic circuits such as inverters, logic gates, etc. In addition, materials such as amorphous Indium-Gallium-Zinc-Oxide (a-IGZO) due to their optical transparency and low deposition temperatures are used in low-cost flexible electronics, which gives the possibility of a-IGZO TFTs in portable electronics for healthcare sensing. The electrical performance of amorphous and microcrystalline transistors made of organic, inorganic and metal oxides materials is determined by the density of states (DOS) in the bandgap of the semiconductor material. In materials such as a-IGZO the DOS is composed of two exponentials describing the tails of acceptor/donor states and two Gaussians representing the deep acceptor/donor states. In this work, simulations were carried out on the density of the deep donor states (N_{GD}) related to the oxygen vacancies (OV) in a-IGZO, the results show that the off current (I_{OFF}) in the transfer curve rises as the density of states of N_{GD} increases due to greater electron density release from OV.

Keywords: amorphous oxide, a-IGZO, thin film transistors, oxygen vacancies, Silvaco.

1. Introduction

Thin Film Transistors (TFTs) made up of mature technology like amorphous silicon (a-Si) have been utilized as switching elements in display panel technologies. However, TFT composed of relative novel semiconductor materials like amorphous oxide semiconductors (AOS) have extended their applications as main elements in logic circuits such as inverters, logic gates, etc. Because amorphous Indium-Gallium-Zinc-Oxide (a-IGZO) is an AOS, it has a wide bandgap ($>3\text{eV}$) [1] and low process temperature [2-4], therefore is widely used in low-cost flexible electronics, which offer significantly improved performance compared to conventional semiconductors. a-IGZO, characterized by its amorphous structure, and high electron mobility (from 10 to 100 $\text{cm}^2/\text{V}\cdot\text{s}$) [5], has emerged as a preferred material for the following applications: integrated logic digital circuit design, touch sensor for flexible and portable devices, gas detection sensing and glucose sensor [5-8]. Other advantages of IGZO are the variety of deposition methods with which it can be obtained, which include: Sputtering, Spin-coated, Atomic layer deposition (ALD) and pulsed layer [4, 9 - 12].

The high field-effect electron mobility in a-IGZO is a consequence of the electronic transport path, which is realized through the overlapping of spherically ns ($n>4$) orbitals. These orbitals, belonging to the metal cation conduction bands [13, 14], are insensitive to the degree of disorder in films; thus, the mobility is almost unaffected by the amorphous phase in the films [15]. One aspect to consider is that a-IGZO has a high intrinsic carrier density ($>10^{17}\text{cm}^{-3}$) [16] due to a great density of free electrons originating from oxygen vacancies. Therefore, it is important to adjust deposition parameters or realize subsequent annealing treatments to achieve an a-IGZO material in which the intrinsic electron concentration can be reduced to a lower level ($<10^{15}\text{cm}^{-3}$), to obtain a low off current and, consequently, a high On/Off current ratio ($I_{\text{ON}}/I_{\text{OFF}}$). Efforts to overcome the above include suppressing the generation of oxygen vacancies [10]. Nonetheless, despite the promising attributes of a-IGZO TFT technology, challenges remain regarding performance and reliability due to sub-gap defects induced by oxygen-vacancy defects.

The electrical performance of amorphous and microcrystalline transistors made of organic, inorganic, and metal oxide materials is determined by the density of states (DOS) in the bandgap of the semiconductor material. In materials such as a-IGZO, the DOS is composed of two exponentials describing the tails of

acceptor/donor states and two Gaussians representing the deep acceptor/donor states [17]. Therefore, it is necessary to carry out simulations of the effects of the density of states within the a-IGZO bandgap and how this affects the transfer and output characteristics. In particular, the effect of the properties of the Al source-drain and DOS, through oxygen vacancies, on the electrical characteristics of a-IGZO TFTs will be simulated. The simulation of the a-IGZO TFT was conducted using the physical properties of semiconductor materials provided by the Silvaco® simulator. The physical structure of the device is achieved through ATHENA®, which simulates fabrication sequences and defines a «mesh» of the device, while the electrical characteristics are obtained by analyzing its DC response using ATLAS®.

2. Experimental part

The a-IGZO TFT was fabricated on a Corning glass substrate (Eagle XG) with a staggered bottom gate contact structure with source and drain top contacts. First, Aluminum (Al) with a thickness of 50 nm was deposited as the gate electrode by e-beam evaporation and patterned by direct lithography, followed by wet etching of Al using a phosphoric solution. Next, as gate dielectric layer, 22 nm of Al_2O_3 was obtained at 150 °C by ALD using precursors such as trimethylaluminum and water. Subsequently, a 15 nm layer of a-IGZO was obtained at room temperature using a Sputtering system operating at 70 W with argon plasma, followed by annealing at 150 °C in air for 1 hour. Then, the gate and dielectric layers were patterned through lithography and solutions of Diluted HCl and a BOE (6:1), respectively. Finally, the drain and source contacts were deposited using 100 nm of Al via sputtering at 150 W in an Ar plasma environment, after those were defined through a lift-off process. The width and channel length of the a-IGZO TFT were 160 μm and 40 μm , respectively. The figure 1 a) and 1 b) shows the top-view and cross section, respectively, of a-IGZO TFT bottom gate structure fabricated in this work.

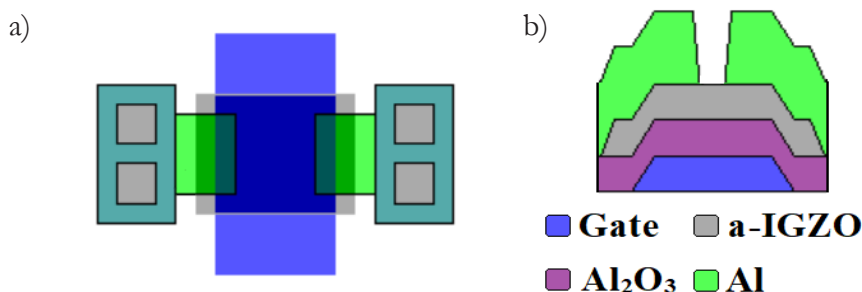


Figure 1. a) Top view and b) cross-section view of staggered bottom gate a-IGZO TFT fabricated.

2.1. Electrical simulation of staggered bottom gate a-IGZO TFTs

We initialize the simulation creating the mesh of staggered bottom gate a-IGZO TFT, it was defined along x-axis from 0 to 70 μm , while y-axis it was from 0 to 1.136 μm , the width and channel length were 160 μm and 40 μm , respectively. Nitride was chosen as mechanical support for a-IGZO TFT. Then, different materials were deposited with the same thickness that these were obtained experimentally, with thickness of 22 nm, 15 nm for Al_2O_3 and a-IGZO, respectively, 50 nm of Al for gate electrode, and 100 nm of Al for source and drain electrodes. Figure 2 shows the a-IGZO TFT cross section generated by ATHENA.

In a-IGZO material the DOS can be described by means of two exponentials representing the density of “tail” states localized near of the valence and conduction band originated from oxygen p-band and metal ions s-band [17], respectively, moreover of two Gaussian distribution indicating the density of deep states. An approximation of the DOS as a function of energy is given by the following expression [18]:

$$g(E) = N_{TA} \exp\left(\frac{E - E_C}{W_{TA}}\right) + N_{GA} \exp\left(-\left(\frac{E_{GA} - E}{W_{GA}}\right)^2\right) + N_{TD} \exp\left(\frac{E_V - E}{W_{TD}}\right) + N_{GD} \exp\left(-\left(\frac{E - E_{GD}}{W_{GD}}\right)^2\right)$$

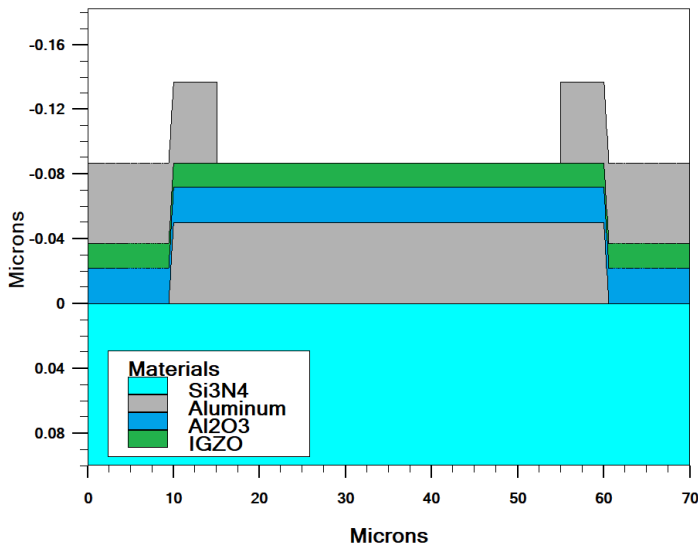


Figure 2. a-IGZO TFT cross section generated by ATHENA.

where N_{TA} and N_{TD} are the density of acceptor/donor tail states from the conduction and valence band, respectively, and W_{TA} and W_{TD} are the slopes of the exponentials representing decay energies of those states. Meanwhile, N_{GA} and N_{GD} are the density of acceptor/donor deep states, respectively, W_{GA} and W_{GD} are the slopes of the Gaussians curves and E_{GA} and E_{GD} are the position of the peaks of energy of those Gaussian distribution in the bandgap. Figure 3 shows the schematic DOS distribution used for a-IGZO TFT simulated at this work. In a-Si TFTs the deep states are originated of dangling bonds [18] and can be represented by two exponential or two Gaussian distributions, when the last are used in the simulations, E_{ga} is placed little above in the middle of E_g , while E_{gd} is placed just below in the middle of E_g . However, for a-IGZO TFTs, deep donor states (N_{GD}) have to be represented by a Gaussian distribution near to the conduction band [17 - 19]. In a-IGZO, deep donor states are originated from oxygen vacancies (OV) which is linked to films with high electron density [18]. The OV model can be written in the following notation [17]: $V_o^x \rightarrow V_o^{+2}$; V_o^x means vacancies of oxygen and those are charged neutral when those are filled and positively charged when are empty. The above expression describes an OV acting like electron donors by removing oxygen bonding [19] when an OV is fully ionized (V_o^{+2}) two electrons ($2e$) are released. Otherwise, deep acceptor states (N_{GA}) are produced by excess of oxygen which is related with low electron density in the films. The oxygen, weakly bonded, capture electron through: $O^0 + e^- \rightarrow O^{-1}$ or $O^{-1} + e^- \rightarrow O^{-2}$ [18]. The acceptor states are neutral when those are unoccupied and negatively charged when are filled by electrons.

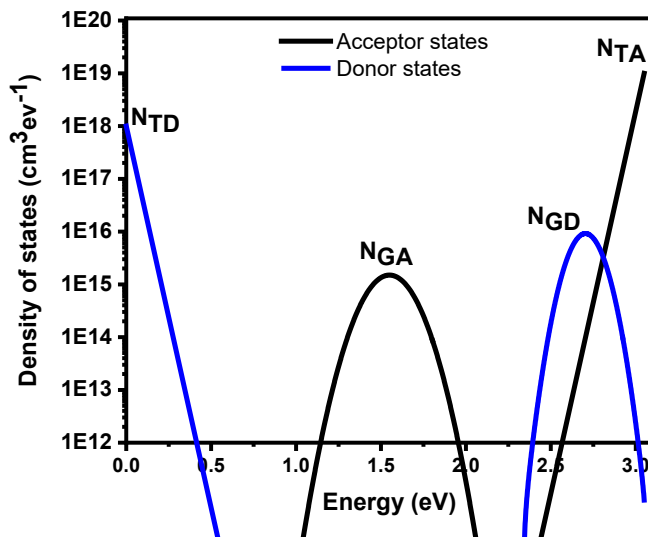


Figure 3. Schematic DOS distribution for a-IGZO.

Kai-Hsiang et al. [18] and Kyun Kim et al. [19] placed N_{GA} just 1.0 eV and 0.5 above valence band, respectively, while Ching Fun et al. [17] not considered deep-gap states in their work. In our simulation deep acceptor-type states and deep donor-type states were collocated at 1.5 eV and 2.8 eV, respectively. Table 1 shows all simulation parameters used in ATLAS® for IGZO TFT. The initial DOS parameters values were set taking into account those reported for a-IGZO in references [17 - 19]. For the simulation, a-IGZO properties like band gap, electron affinity and permittivity were set according to the default values provided by ATLAS® [20], while a field electron mobility of 8.9 cm²/V·s extracted experimental of our a-IGZO TFT fabricated was considered. Moreover, firstly a work-function of 4.2 eV for gate, source and drain contacts was set in the simulation. The DOS parameters values that fitted the simulated and experimental transfer (ID vs VGS) and output (ID vs VDS) curves of a-IGZO TFT were: $N_{TA} = 2 \times 10^{19} \text{ cm}^{-3} \text{ eV}^{-1}$, $N_{GD} = 1 \times 10^{18} \text{ cm}^{-3} \text{ eV}^{-1}$, $N_{GA} = 1.5 \times 10^{18} \text{ cm}^{-3} \text{ eV}^{-1}$, $N_{GA} = 1.5 \times 10^{18} \text{ cm}^{-3} \text{ eV}^{-1}$, $N_{GD} = 1.5 \times 10^{18} \text{ cm}^{-3} \text{ eV}^{-1}$, $W_{TA} = 0.02 \text{ eV}$, $W_{TD} = 0.02 \text{ eV}$. Figure 4 a) presents the simulated and experimental transfer curve of a-IGZO TFT. The experimental curve was measured using the Keithley 4200 semiconductor analyzer (DC resolution of 10⁻¹⁸ A and 0.2 μV), sweeping the gate voltage from -1 to 5 V and then reversing it, both with steps of 0.1 V. As can be seen the simulated graph reproduces well the experimental transfer curve in saturation region ($V_{DS} = 5\text{V}$). However, in Figure 4 b), we can observe that simulated output curve doesn't matches the experimental output curve in low drain voltages ($V_{DS} < 0.5\text{V}$) and for $V_{GS} = 5\text{V}$. The last may be due to

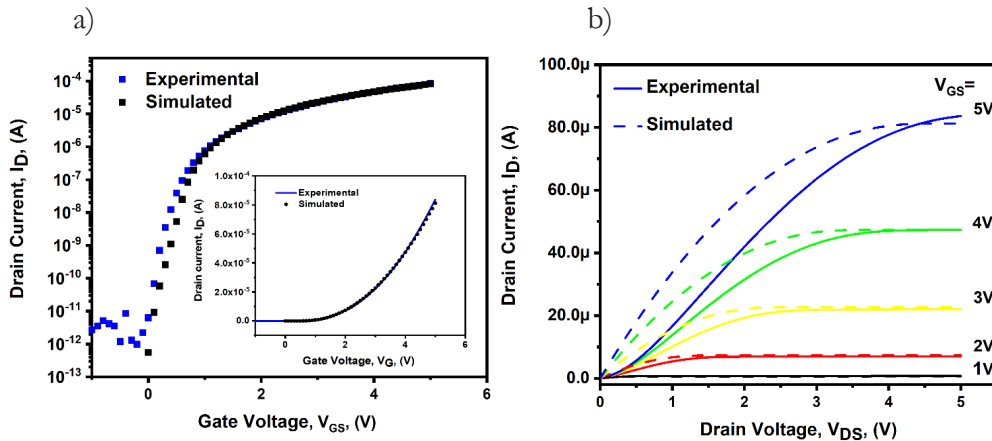


Figure 4. a) Simulated and experimental transfer curves and b) output curve of a-IGZO TFT.

initially the simulation has been realized with a work-function of Al contacts near to electron affinity value of a-IGZO, and according to the expression [21]: $q\theta_B = q(\Phi_m - \chi_s)$; where θ_B is the Schottky barrier height, Φ_m is the work-function of metal (Al=4.2 eV), χ_s is the electron affinity of semiconductor (IGZO= 4.16 eV) and q is the electron charge; $q\theta_B = 0.04 eV$, therefore in the simulated output graph we have ohmic contacts. However, due to interface states between Al and a-IGZO, the experimental work-function of Al is higher than 4.2 eV, then $q\theta_B$ too will be greater, thus presenting Schottky contacts and a non-linear relation between I_D and V_{DS} as can we see in Figure 4 b).

2.2. Effect of work-function S/D Al-contacts

To fit the simulated and experimental output curves, we need to increase work-function of Source/Drain (S/D) Al-contacts until a non-ohmic contact is present in the simulated graph. First, we assign a work-function of S/D Al-contacts of 4.7 eV keeping the DOS parameters unchanged relative to previous simulation. Figure 5 a) shows the simulated output graph with a work-function S/D Al-contact of 4.7 eV. As can we notice, a Schottky contact is achieved in the output curves and then fitting better both graphs in lows values of V_{DS} . However, by increasing the work-function has decreased the maximum drain current to 64 μA in comparison to 81 μA got in previous simulation with a work-function of 4.2 eV. The above is due to the fact that simulation has been realized unaffected the DOS, therefore is necessary to carry out simulation varying DOS and observe how this affect the transfer and output graphs. If we observe the initial DOS parameters (Table 1) we can see that conduction band tail slope (W_{TA}) value (0.1 eV) is well above of 0.011 eV and 0.012 eV reported in [18] and [17] respectively. Then simulations were performed varying W_{TA} parameter until the simulation graphs had a better fit. Figure 5b) shows both output curves where can be seen that I_D has increased near of value of I_D achieved experimentally. To understand the physical origin of this increase we have plotted contour graph of electron concentration (n), in saturation region, when W_{TA} is 0.1 eV Figure 6a) and 0.020 eV, Figure 6c). We can notice in Figure 6c) that maximum n ($3.6 \times 10^{19} \text{ cm}^{-3}$) is slightly larger than the maximum n ($3.1 \times 10^{19} \text{ cm}^{-3}$) when W_{TA} is 0.1 eV (Figure 5a), however in the former the minimum n ($1.5 \times 10^{17} \text{ cm}^{-3}$) is almost an order of magnitude larger that when W_{TA} is 0.1 eV ($3.4 \times 10^{16} \text{ cm}^{-3}$). The above is due with a higher W_{TA} there are a larger tail acceptor-states therefore part of free electrons are trapped in these states and reducing I_D . Additionally, in Figures 6b) and d) we have plotted electron concentration and

Parameter	Values	Description
N_{TA}	$1.0 \times 10^{19} \text{ cm}^{-3} \text{ eV}^{-1}$	Acceptor tail states density
N_{TD}	$1.0 \times 10^{18} \text{ cm}^{-3} \text{ eV}^{-1}$	Donor tail states density
W_{TA}	0.1 eV	Slope energy of acceptor tail states
W_{TD}	0.02 eV	Slope energy of donor tail states
N_{GA}	$1.5 \times 10^{18} \text{ cm}^{-3} \text{ eV}^{-1}$	Acceptor deep states density
N_{GD}	$1.0 \times 10^{17} \text{ cm}^{-3} \text{ eV}^{-1}$	Donor deep states density
W_{GA}	0.14 eV	Slope energy of acceptor deep states
W_{GD}	0.07 eV	Slope energy of donor deep states
E_{GA}	1.5 eV	Peak energy of acceptor deep states
E_{GD}	2.8 eV	Peak energy of donor deep states
n_i (a-IGZO)	$7 \times 10^{11} \text{ cm}^{-2}$	Intrinsic carrier concentration in TFT channel
E_g (a-IGZO)	3.1 eV	Band gap
Permittivity (a-IGZO)	9	Dielectric constant
Nc	$5 \times 10^{18} \text{ cm}^{-3} \text{ eV}^{-1}$	Density of states for conduction band
Nv	$5 \times 10^{21} \text{ cm}^{-3} \text{ eV}^{-1}$	Density of states for Valence band
	$8.9 \text{ cm}^2 / \text{V} \cdot \text{s}$	Electron mobility
SRH	Activated	Shockley-Read-Hall recombination
UST	Activated	Universal Schottky Tunneling Model
TRAP. TUNNEL	Activated	Trapp-assisted Tunneling
TRAP. COULOMBIC	Activated	Poole-Frenkel barrier lowering for coulombic wells will used for traps
TAUN0	1×10^{-6}	SRH lifetimes for electrons
TAUP0	1×10^{-6}	SRH lifetimes for holes
D.TUNNEL	1×10^{-6}	Maximum tunneling distance used for the UST model
ME.TUNNEL	0.2	Electron effective mass used for the UST model

Table 1. Initial parameters used in ATLAS® for a-IGZO TFT simulation.

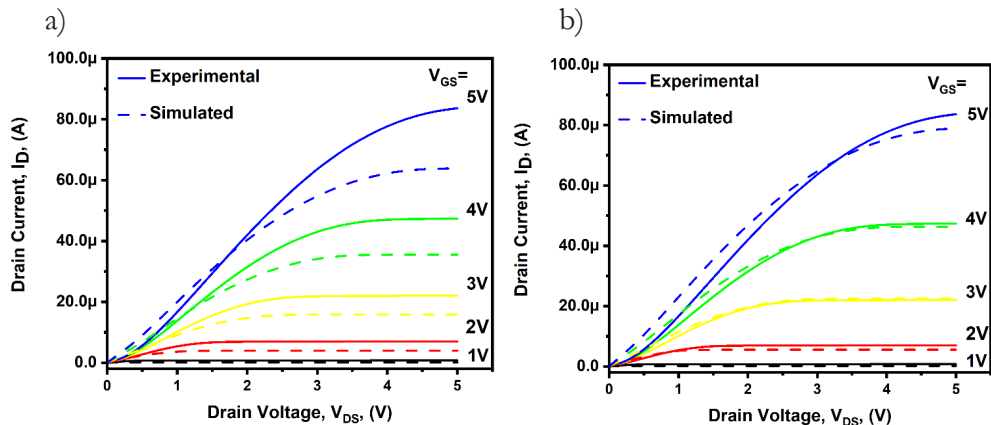


Figure 5. Output graphs with a workfunction of Source/Drain contacts of 4.7 eV and a) $W_{TA} = 0.1$ eV and b) $W_{TA} = 0.020$ eV.

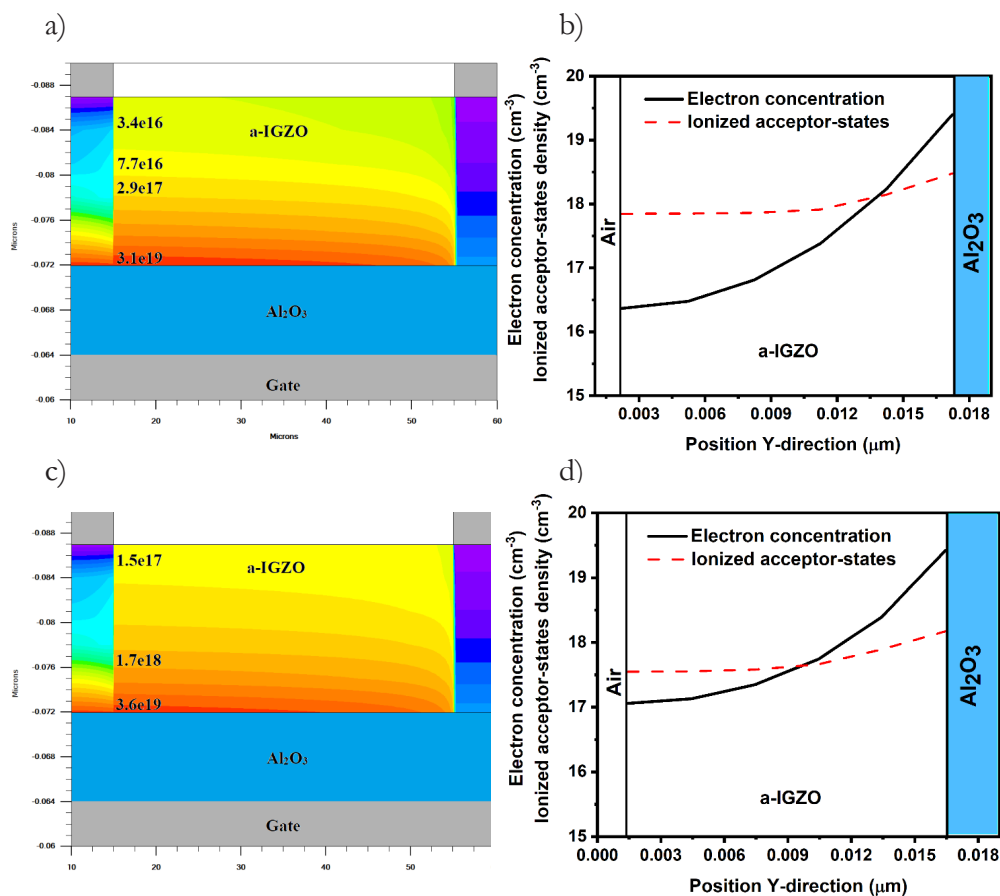


Figure 6. Contour graph of electron concentration for a) $W_{TA} = 0.1$ eV and c) $W_{TA} = 20$ meV; electron concentration and ionized acceptor-states density for b) $W_{TA} = 0.1$ eV and b) $W_{TA} = 20$ meV.

the ionized acceptor-states. We can observe in Figure 6b) that there are more ionized acceptor-states with respect of ionized acceptor-states in figure 6 d), as a consequence of a higher W_{TA} in former. The acceptor-states are ionized when are occupied with electrons, thus if more traps have been ionized, then the total electron concentration in a-IGZO channel is lower.

2.3. Effect of Vacancies of Oxygen

Figure 7a) shows the characteristic transfer curves in saturation region ($V_{DS} = 5V$) for different deep donor-states densities (N_{GD}) varying from $1 \times 10^{16} \text{ cm}^{-3}$ to $1 \times 10^{18} \text{ cm}^{-3}$ and fixing the Gaussian peak energy position in 2.8 eV in the bandgap, all other DOS parameter has been keeping constants during the simulations. As can be seen, an increasing of N_{GD} from $1 \times 10^{16} \text{ cm}^{-3}$ to $1 \times 10^{18} \text{ cm}^{-3}$ decreases the I_{ON}/I_{OFF} ratio (5.2×10^7) practically two orders of magnitude (7.7×10^5) by means increasing I_{OFF} current by the same amount and keeping the maximum I_{ON} current unaffected. Moreover, a subthreshold slope values of 65 meV and 185 meV for N_{GD} of 1×10^{16} and 1×10^{18} , respectively, were extracted of simulations. In order to clarify the reduction of I_{ON}/I_{OFF} with increased of N_{GD} , we have plotted in figure 7 b) both the ionized donor states density (N_{GD}^+) and electron concentration in off condition of a-IGZO TFT (i.e. $V_{GS} = V_{DS} = 0V$). We can notice that N_{GD}^+ for $N_{GD} = 1 \times 10^{18}$ is higher than N_{GD}^+ for $N_{GD} = 1 \times 10^{16}$ practically for two orders of magnitude, thus the electron concentration has risen 10^{12} to 10^{14} cm^{-3} . As was

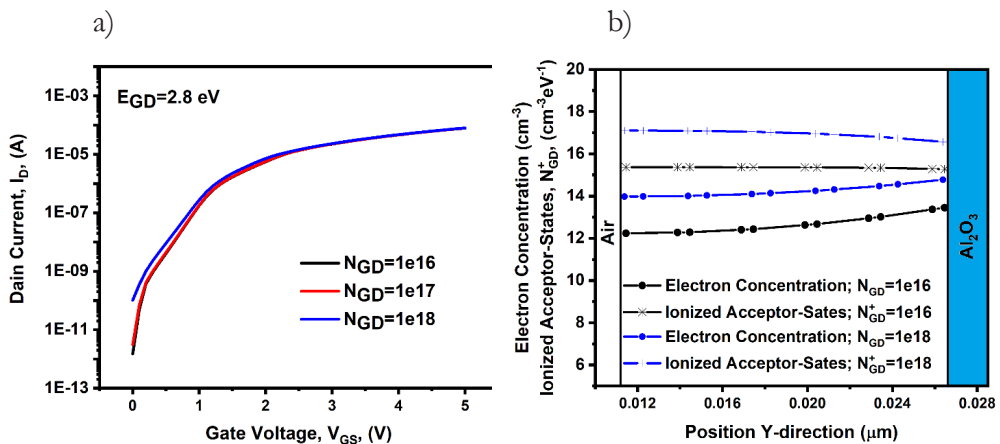


Figure 7. a) Transfer curve in saturation region for $N_{GD} = 1 \times 10^{16}$ to $1 \times 10^{18} \text{ cm}^{-3}$ keeping $E_{GD} = 2.8$ eV near of conduction band; b) electron concentration and ionized acceptor states to $N_{GD} = 1 \times 10^{16}$ and $1 \times 10^{18} \text{ cm}^{-3} \text{ eV}^{-1}$.

mentioned early, N_{GD} is related with oxygen vacancies which when ionized are empty and acting as electron donors, therefore lowering the I_{ON}/I_{OFF} ratio for a higher N_{GD} . The mechanism of increment of electron concentration, in off condition, related with vacancies of oxygen is called “auto-doping”.

3. Conclusions

In this work, we have performed simulations of a-IGZO TFT based on the physical properties of different materials that comprise the TFT, such as the work function of the source and drain (S/D) contacts and the density of states through oxygen vacancies (OV) in a-IGZO. The results of our simulations show that when the work function of Al is considered, there is a reduction of drain current (less than an order of magnitude) and non-linear relation of ID vs VGS due Schottky contacts present in the S/D contacts. On the other hand, the oxygen vacancies are modeled by the density of deep-donors states (NGD) near the conduction band, the simulation shows that an excess of OV generates a large density of free electrons when the TFT is off, thus decreasing the I_{ON}/I_{OFF} ratio up two orders of magnitude when the TFT is in the saturation region. Finally, the simulation results show that the device does not present a good interface between the metal and the a-IGZO, which decreased the drain current.

References

1. Mativenga, M. (2021, December). Highly stable thin-film transistors for flexible and transparent displays. *2021 International Conference on Electrical, Computer, and Energy Technologies (ICECET)*, 1–6.
<https://doi.org/10.1109/ICECET52533.2021.9698710>
2. Zhang, S., et al. (2024, January). Reduction of internal stress in InGaZnO (IGZO) thin-film transistors by ultra-thin metal oxide layer. *Materials Science in Semiconductor Processing*, 173, 108093.
<https://doi.org/10.1016/j.mssp.2023.108093>
3. Lin, C., Fang, Y., Chang, W., Chiou, M., & Chen, C. (2014). Effect of gate barrier and channel buffer layer on electric properties and transparency of the a-IGZO thin-film transistor. *Microelectronics Reliability*, 54(5), 905–910.
<https://doi.org/10.1016/j.microrel.2014.01.015>
4. Toledo, P., Hernandez, I. S., & Hernandez-Cuevas, F. (2023, July). Electrical instabilities of a-IGZO TFTs under different conditions of bias and illumination stress. *Microelectronics Reliability*, 148, 115186.
<https://doi.org/10.1016/j.microrel.2023.115186>
5. Eadi, S. B., et al. (2022). Indium-gallium-zinc oxide (IGZO) thin-film gas sensors prepared via post-deposition high-pressure annealing for NO₂ detection. *Sensors and Actuators B: Chemical*, 353(2), 131082.
<https://doi.org/10.1016/j.snb.2021.131082>
6. Kim, J., et al. (2020, July). Effect of IGZO thin films fabricated by pulsed-DC and RF sputtering on TFT characteristics. *Materials Science in Semiconductor Processing*, 120, 105264.
<https://doi.org/10.1016/j.mssp.2020.105264>
7. Du, X., & Herman, G. S. (2018). Transparent In-Ga-Zn-O field-effect glucose sensors fabricated directly on highly curved substrates. *Sensors and Actuators B: Chemical*, 268, 123–128.
<https://doi.org/10.1016/j.snb.2018.04.087>
8. Kim, J. S., et al. (2017). Dynamic logic circuits using a-IGZO TFTs. *IEEE Transactions on Electron Devices*, 64(10), 4123–4130.
<https://doi.org/10.1109/TED.2017.2738665>
9. Sahoo, A. K., & Wu, G. M. (2016). Effects of argon flow rate on electrical properties of amorphous indium gallium zinc oxide thin-film transistors. *Thin Solid Films*, 605, 129–135.
<https://doi.org/10.1016/j.tsf.2015.12.016>
10. Xu, W., et al. (2018). Low-temperature solution-processed IGZO thin-film transistors. *Applied Surface Science*, 455, 554–560.
<https://doi.org/10.1016/j.apsusc.2018.06.005>

11. Cho, M. H., et al. (2018). High-performance amorphous indium gallium zinc oxide thin-film transistors fabricated by atomic layer deposition. *IEEE Electron Device Letters*, 39(5), 688–691.
<https://doi.org/10.1109/LED.2018.2812870>
12. Chen, J., Wang, L., & Su, X. (2012). InGaZnO thin films grown by pulsed laser deposition. *Vacuum*, 86(9), 1313–1317.
<https://doi.org/10.1016/j.vacuum.2011.12.001>
13. Zhou, F., et al. (2012). Top-gate amorphous IGZO thin-film transistors with a SiO buffer layer inserted between active channel layer and gate insulator. *Current Applied Physics*, 12, 228–232.
<https://doi.org/10.1016/j.cap.2011.06.006>
14. Hernandez-Luna, I. S., Toledo, P., Hernandez-Cuevas, F., & Hernandez-Como, N. (2023). Reliability of flexible amorphous In-Ga-Zn-O (a-IGZO) thin-film transistors. *Research Advances in Nanosciences, Micro and Nanotechnologies*, IV, 249–262.
15. Kamiya, T., & Hosono, H. (2010, January). Material characteristics and applications of transparent amorphous oxide semiconductors. *NPG Asia Materials*, 2, 15–22.
<https://doi.org/10.1038/asiamat.2010.5>
16. Nomura, K., Takagi, A., Kamiya, T., Ohta, H., Hirano, M., & Hosono, H. (2006). Amorphous oxide semiconductors for high-performance flexible thin-film transistors. *Japanese Journal of Applied Physics, Part 1: Regular Papers, Short Notes and Review Papers*, 45(5B), 4303–4308.
<https://doi.org/10.1143/JJAP.45.4303>
17. Fung, T., Chuang, C., Chen, C., Abe, K., & Cottle, R. (2009, November). Two-dimensional numerical simulation of radio-frequency sputter amorphous In-Ga-Zn-O thin-film transistors. *Journal of Applied Physics*, 15.
<https://doi.org/10.1063/1.3234400>
18. Yu, E., Kim, T. O., & Kanicki, J. (2014). Density of states of amorphous In-Ga-Zn-O from electrical and optical characterization. *Journal of Applied Physics*, 116.
<https://doi.org/10.1063/1.4898567>
19. Kim, D. K., Park, J., Zhang, X., Park, J., & Bae, J. H. (2020). Numerical study of sub-gap density of states dependent electrical characteristics in amorphous In-Ga-Zn-O thin-film transistors. *Electronics*, 9(10), 1652.
<https://doi.org/10.3390/electronics9101652>
20. Silvaco International Inc. (2016). *Atlas User's Manual: Device Simulation Software*.
21. Kano, K. (1998). *Semiconductor Devices*. Prentice Hall.